

## Pharmacophore Assessment Through 3-D QSAR: evaluation of the predictive ability on new derivatives by the application on a serie of antitubercularagents.

Rino Ragno, and Flavio Ballante

*J. Chem. Inf. Model.*, **Just Accepted Manuscript** • DOI: 10.1021/ci400132q • Publication Date (Web): 25 Apr 2013

Downloaded from <http://pubs.acs.org> on April 28, 2013

### Just Accepted

“Just Accepted” manuscripts have been peer-reviewed and accepted for publication. They are posted online prior to technical editing, formatting for publication and author proofing. The American Chemical Society provides “Just Accepted” as a free service to the research community to expedite the dissemination of scientific material as soon as possible after acceptance. “Just Accepted” manuscripts appear in full in PDF format accompanied by an HTML abstract. “Just Accepted” manuscripts have been fully peer reviewed, but should not be considered the official version of record. They are accessible to all readers and citable by the Digital Object Identifier (DOI®). “Just Accepted” is an optional service offered to authors. Therefore, the “Just Accepted” Web site may not include all articles that will be published in the journal. After a manuscript is technically edited and formatted, it will be removed from the “Just Accepted” Web site and published as an ASAP article. Note that technical editing may introduce minor changes to the manuscript text and/or graphics which could affect content, and all legal disclaimers and ethical guidelines that apply to the journal pertain. ACS cannot be held responsible for errors or consequences arising from the use of information contained in these “Just Accepted” manuscripts.

1  
2  
3  
4  
5  
6 **Pharmacophore Assessment Through 3-D QSAR: evaluation of the predictive ability on new**  
7  
8 **derivatives by the application on a serie of antitubercular agents.**  
9

10  
11 Laura Friggeri,<sup>§,†</sup> Flavio Ballante,<sup>\*,§,‡</sup> Rino Ragno,<sup>\*,‡</sup> Ira Musmuca,<sup>‡</sup> Daniela De Vita,<sup>†</sup> Fabrizio  
12 Manetti,<sup>□</sup> Mariangela Biava,<sup>†</sup> Luigi Scipione,<sup>†</sup> Roberto Di Santo,<sup>+,†</sup> Roberta Costi,<sup>+,†</sup> Marta  
13 Feroci,<sup>^</sup> and Silvano Tortorella.<sup>†</sup>  
14  
15

16  
17 <sup>‡</sup>Rome Center for Molecular Design, Dipartimento di Chimica e Tecnologie del Farmaco, Sapienza  
18 Università di Roma, P. le A. Moro 5, 00185 Roma, Italy.  
19

20 <sup>†</sup>Dipartimento di Chimica e Tecnologie del Farmaco, Sapienza Università di Roma, P. le A. Moro  
21 5, 00185 Roma, Italy.  
22

23 <sup>+</sup>Istituto Pasteur-Fondazione Cenci Bolognetti, Dipartimento di “Chimica e Tecnologie del  
24 Farmaco”, “Sapienza” Università di Roma, P.le A. Moro 5, 00185 Rome, Italy

25 <sup>□</sup>Dipartimento di Biotecnologie, Chimica e Farmacia, Università degli Studi di Siena, Via Aldo  
26 Moro 2, I-53100 Siena, Italy.

27 <sup>^</sup>Dipartimento di Scienze di Base e Applicate per l’Ingegneria, Sapienza University of Rome, Via  
28 Castro Laurenziano 7, I-00161 Rome, Italy.  
29

30  
31 <sup>§</sup>*L.F. and F.B. contributed equally to this work*  
32  
33  
34  
35  
36  
37  
38  
39  
40  
41  
42  
43  
44  
45  
46  
47  
48  
49  
50  
51  
52  
53  
54  
55  
56  
57  
58  
59  
60

**Abstract**

Pharmacophoric mapping is a useful procedure to frame, especially when crystallographic receptor structures are unavailable as in ligand-based studies, the hypothetical site of interaction. In this study, 71 pyrrole derivatives active against *M. tuberculosis* were used to derive through a recent new 3-D QSAR protocol, 3-D QSAutogrid/R, several predictive 3-D QSAR models on compounds aligned by a previously reported pharmacophoric application. A final multi probe (MP) 3-D QSAR model was then obtained configuring itself as a tool to derive pharmacophoric quantitative models. To stress the applicability of the described models, an external test set of unrelated and newly synthesized series of R-4-amino-3-isoxazolidinone derivatives found to be active at micromolar level against *M. tuberculosis*, was used and the predicted bioactivities were in good agreement with the experimental values. The 3-D QSAutogrid/R procedure proved to be able to correlate by a single multi-informative scenario the different activity molecular profiles thus confirming its usefulness in the rational drug design approach.

## 1. Introduction

Tuberculosis (TB), an infectious disease mainly caused by *Mycobacterium tuberculosis* (Mtb), remains a major public health problem and causes ill-health among millions of people each year. TB ranks as the second leading cause of death from an infectious disease worldwide, after the human immunodeficiency virus (HIV-1). The 2012WHO Global tuberculosis report estimates there are almost 9 million new cases and 1.4 million TB deaths.<sup>1</sup> Moreover, two billion people are estimated to be latently infected with Mtb, and the 10% of them reactivating to active TB with major risk relative to immigrants from endemic areas, people with HIV-1 infection, individuals with underlying diseases (silicosis, diabetes mellitus, malignant conditions).<sup>2</sup>

Currently, the standard treatment comprises: first line drugs, such as isoniazid (INH), pyrazinamide (PZA), ethambutol (EMB), rifampin (RIF); and second line drugs, such as ethionamide (ETH), p-aminosalicylic acid (PAS), capreomycin, aminoglycosides, D-cycloserine (DCS) and fluoroquinolones.<sup>3</sup>

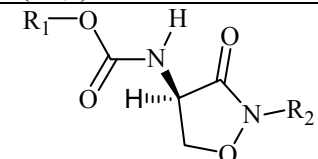
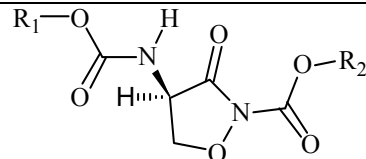
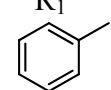
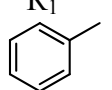
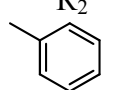
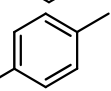
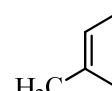
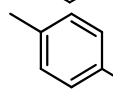
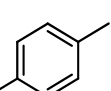
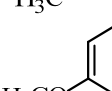
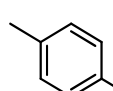
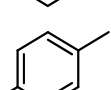
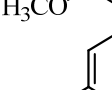
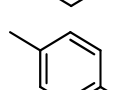
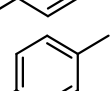
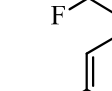
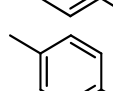
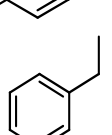
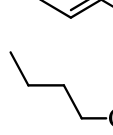
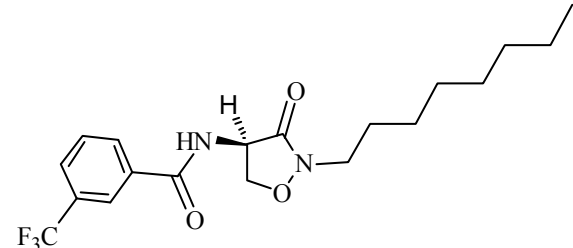
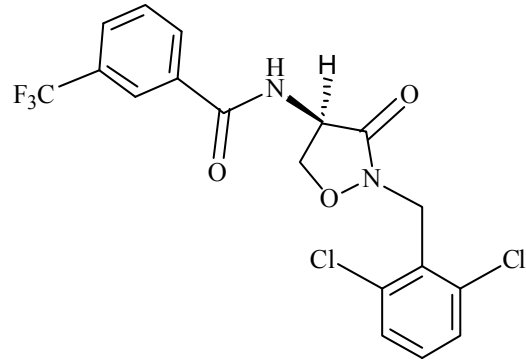
The required long-term drug treatment, due to the high persistence of Mtb, combined with poor compliance of the patients, highly contributes to develop drug resistant strains, particularly multidrug-resistant (MDR, resistant at least to INH and RIF) and extensively drug-resistant (XDR, resistant at least to INH, RIF and three of second line class of anti-TB drugs). Recently a more dangerous form of bacilli, named totally drug-resistant (TDR) showing *in vitro* resistance to all first- and second –line drugs tested have been isolated.<sup>4,5</sup>

To reduce this increasing problem, antitubercular drugs are used with specific therapeutic protocols under direct observation therapy short course (DOTS) conditions.<sup>6</sup>

The need for new shorter therapeutic regimens and new classes of drugs active on MDR, XDR and TDR MTB drives pharmaceutical research to accelerate in the development process of new anti-TB drugs.<sup>7</sup> Continuing our research on anti-TB agents,<sup>8,9</sup> here we report the assessment of a previously reported pharmacophore model<sup>10</sup> through 3-D QSAutogrid/R, a recent introduced quantitative ligand-based design protocol.<sup>11</sup> The developed 3-D QSAR models were tested for their predictive

ability on a series of new independently synthesized R-4-amino-3-isoxazolidinone derivatives **1a-e**, **2a-f** and **3h-i** (Table 1). These compounds have been designed to evaluate the effects on antitubercular activity due by the introduction of acyl substituents on N(2) atom of oxoisoxazolidine ring and on amino group.

**Table 1.** R-4-amino-3-isoxazolidinone derivatives: monocarbamates (**1a-e**), dicarbamates (**2a-f**) and amides (**3h,i**).

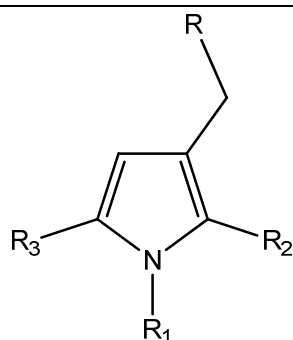
 Monocarbamates <b>1a-e</b>			 Dicarbamates <b>2a-f</b>		
#	R <sub>1</sub>	R <sub>2</sub>	#	R <sub>1</sub>	R <sub>2</sub>
<b>1a</b>		H	<b>2a</b>		
<b>1b</b>		H	<b>2b</b>		
<b>1c</b>		H	<b>2c</b>		
<b>1d</b>		H	<b>2d</b>		
<b>1e</b>		H	<b>2e</b>		
			<b>2f</b>		
 <b>3h</b>			 <b>3i</b>		
Amides <b>3h, 3i</b>					

## 2 Results and Discussion

### 2.1 Ligand-Based Design

A first pharmacophore model for anti-TB activity was previously developed by us<sup>12</sup> using a series of 32 imidazole derivatives with interesting antitubercular activity, adopting the HipHop<sup>13</sup> method. The final model was then optimized<sup>14</sup> and finally characterized by four pharmacophoric features as follows: an hydrogen bond acceptor feature (HBA), two aromatic ring features (RA1, RA2), and an hydrophobic feature (HY); and applied recently to different antimycobacterial agents.<sup>10, 15</sup> Even if this model is able to describe the needed structural properties for antitubercular activity and identify the possible antimycobacterial candidates within large molecular databases, it doesn't permit to correlate quantitatively biological activity of the compounds with their structural features. This limitation is due to the fact that the model was obtained by application of the qualitative approach referred to as the common feature hypothesis generation method. In addition, as for the specific case of the newly synthesized monocarbamates (**1a-e**), dicarbamates (**2a-f**) and amides (**3h-i**) of R-4-amino-3-isoxazolidinone (Figure 1, discussion in the External Test Set Prediction Analysis paragraph), a proper evaluation may be difficult when a partial overlap of the investigated compounds with the defined pharmacophore areas is established. In this perspective the use of a three-dimensional quantitative approach is useful and several 3-D QSAR PLS models, characterized by a training set (Table 2, Table S1 for numeric reference) of 71 published antitubercular agents,<sup>10, 15-19</sup> were built through the 3-D QSAutogrid/R<sup>11</sup> protocol: 8 mono-probe (see Table S5 for probes' definition) 3-D QSAR PLS models were generated and optimized via the CAPP<sup>11</sup> procedure (Table 3 and 4) and a final multi probe (MPGRS) model (Tables 5 and S5) was then derived to correlate the pharmacophoric features required for antitubercular activity with molecular structures. Activity data, originally determined as MIC ( $\mu\text{g/mL}$ ) values, were transformed to pMIC values on molar basis.

**Table 2.** Structure and antimycobacterial activity against *M. tuberculosis* 103471 of the pyrrole derivatives used as training set for the generation of the 3-D QSAR models



compd <sup>a</sup>	R <sup>b</sup>	R <sub>1</sub>	R <sub>2</sub>	R <sub>3</sub>	pMIC <sup>c</sup>
1	B	2-F-Ph	CH <sub>3</sub>	2-F-Ph	4.68
2	A	2-Cl-Ph	CH <sub>3</sub>	2-F-Ph	5
3	B	2-Cl-Ph	CH <sub>3</sub>	2-F-Ph	4.09
4	A	2-F-Ph	CH <sub>3</sub>	2-Cl-Ph	5
5	B	2-F-Ph	CH <sub>3</sub>	2-Cl-Ph	4.4
6	A	2-Cl-Ph	CH <sub>3</sub>	2-Cl-Ph	5.02
7	B	2-Cl-Ph	CH <sub>3</sub>	2-Cl-Ph	4.41
8	A	2-F-Ph	CH <sub>3</sub>	α-naphthyl	4.11
9	B	2-F-Ph	CH <sub>3</sub>	α-naphthyl	4.11
10	A	2-Cl-Ph	CH <sub>3</sub>	α-naphthyl	4.13
11	B	2-Cl-Ph	CH <sub>3</sub>	α-naphthyl	4.13
12	A	α-naphthyl	CH <sub>3</sub>	2-Cl-Ph	4.13
13	B	4-F-Ph	CH <sub>3</sub>	Ph	4.36
14	B	Ph	CH <sub>3</sub>	4-F-Ph	4.36
15	A	4-Cl-Ph	CH <sub>3</sub>	4-F-Ph	5.30
16	B	4-F-Ph	CH <sub>3</sub>	4-F-Ph	4.47
17	A	4-F-Ph	CH <sub>3</sub>	4-F-Ph	5.58
18	B	4-F-Ph	CH <sub>3</sub>	4-Cl-Ph	5.30
19	A	4-F-Ph	CH <sub>3</sub>	4-Cl-Ph	5.60
20	A	2-F-Ph	CH <sub>3</sub>	Ph	4.66
21	B	2-F-Ph	CH <sub>3</sub>	Ph	4.06

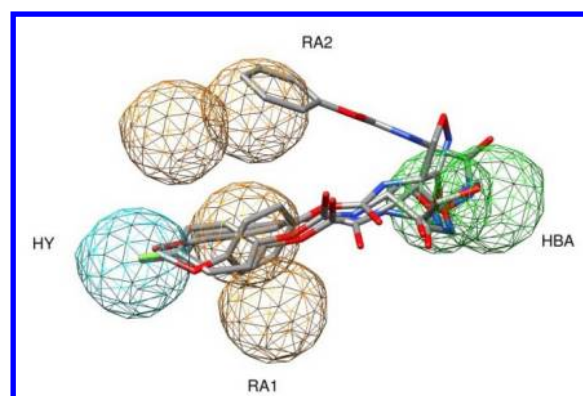
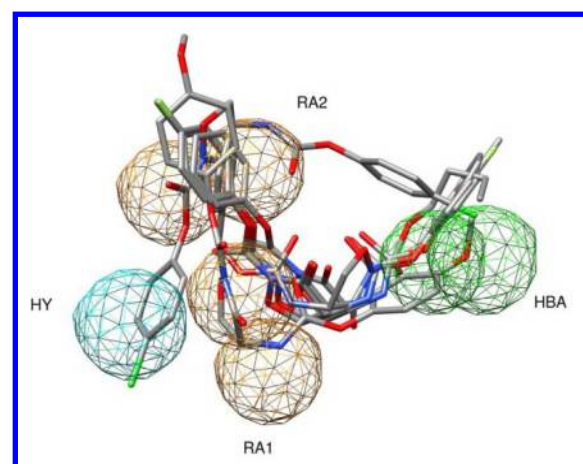
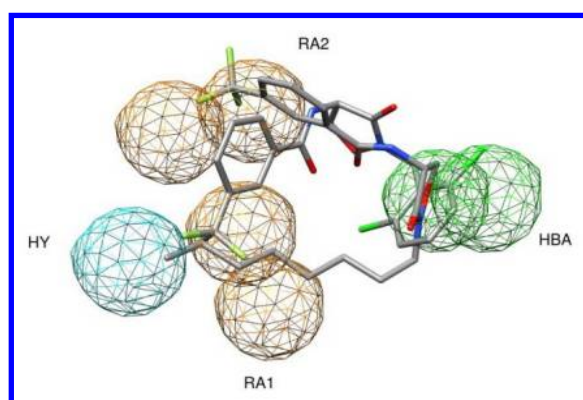
1						
2						
3	22	A	Ph	CH <sub>3</sub>	2-F-Ph	4.96
4						
5	23	B	Ph	CH <sub>3</sub>	2-F-Ph	4.36
6						
7	24	A	2-Cl-Ph	CH <sub>3</sub>	Ph	4.38
8						
9	25	B	2-Cl-Ph	CH <sub>3</sub>	Ph	4.07
10						
11	26	B	Ph	CH <sub>3</sub>	2-Cl-Ph	4.07
12						
13	27	A	$\alpha$ -naphthyl	CH <sub>3</sub>	Ph	4.1
14						
15	28	B	$\alpha$ -naphthyl	CH <sub>3</sub>	Ph	4.09
16						
17	29	A	Ph	CH <sub>3</sub>	$\alpha$ -naphthyl	4.10
18						
19	30	B	Ph	CH <sub>3</sub>	$\alpha$ -naphthyl	4.09
20						
21	31	B	Ph	CH <sub>3</sub>	Ph	4.33
22						
23	32	A	4-F-Ph	CH <sub>3</sub>	2-Cl-Ph	5.00
24						
25	33	B	4-F-Ph	CH <sub>3</sub>	2-Cl-Ph	4.70
26						
27	34	B	4-F-Ph	CH <sub>3</sub>	2-F-Ph	4.08
28						
29	35	A	4-F-Ph	CH <sub>3</sub>	4-CH <sub>3</sub> -Ph	5.98
30						
31	36	B	4-F-Ph	CH <sub>3</sub>	3-CH <sub>3</sub> -Ph	4.37
32						
33	37	A	4-F-Ph	CH <sub>3</sub>	2-CH <sub>3</sub> -Ph	4.98
34						
35	38	B	4-F-Ph	CH <sub>3</sub>	2-CH <sub>3</sub> -Ph	4.07
36						
37	39	A	4-F-Ph	CH <sub>3</sub>	2,4-Cl <sub>2</sub> -Ph	5.34
38						
39	40	B	4-F-Ph	CH <sub>3</sub>	2,4-F <sub>2</sub> -Ph	5.00
40						
41	41	A	2-Cl-Ph	CH <sub>3</sub>	4-F-Ph	5.30
42						
43	42	B	2-Cl-Ph	CH <sub>3</sub>	4-F-Ph	5.00
44						
45	43	B	2-F-Ph	CH <sub>3</sub>	4-F-Ph	4.68
46						
47	44	A	4-CH <sub>3</sub> -Ph	CH <sub>3</sub>	4-F-Ph	5.58
48						
49	45	A	3-CH <sub>3</sub> -Ph	CH <sub>3</sub>	4-F-Ph	4.98
50						
51	46	B	3-CH <sub>3</sub> -Ph	CH <sub>3</sub>	4-F-Ph	4.40
52						
53	47	A	2-CH <sub>3</sub> -Ph	CH <sub>3</sub>	4-F-Ph	4.68
54						
55	48	B	2-CH <sub>3</sub> -Ph	CH <sub>3</sub>	4-F-Ph	4.10
56						
57	49	A	2,4-Cl <sub>2</sub> -Ph	CH <sub>3</sub>	4-F-Ph	5.64
58						
59	50	B	2,4-Cl <sub>2</sub> -Ph	CH <sub>3</sub>	4-F-Ph	5.03
60						
	51	A	2,4-F <sub>2</sub> -Ph	CH <sub>3</sub>	4-F-Ph	5.30

1						
2						
3	52	B	2,4-F <sub>2</sub> -Ph	CH <sub>3</sub>	4-F-Ph	4.40
4						
5	53	A	4-F-Ph	CH <sub>3</sub>	4-C <sub>2</sub> H <sub>5</sub> -Ph	5.60
6						
7	54	A	4-F-Ph	CH <sub>3</sub>	4- <i>i</i> -propyl-Ph	6.21
8						
9	55	A	4-C <sub>2</sub> H <sub>5</sub> -Ph	CH <sub>3</sub>	4-F-Ph	5.30
10						
11	56	A	4-C <sub>3</sub> H <sub>7</sub> -Ph	CH <sub>3</sub>	4-F-Ph	5.61
12						
13	57	A	4-Cl-Ph	CH <sub>3</sub>	4-CH <sub>3</sub> -Ph	5.90
14						
15	58	A	4-Cl-Ph	CH <sub>3</sub>	4-C <sub>2</sub> H <sub>5</sub> -Ph	6.22
16						
17	59	A	4-Cl-Ph	CH <sub>3</sub>	4-C <sub>3</sub> H <sub>7</sub> -Ph	6.23
18						
19	60	A	4-Cl-Ph	CH <sub>3</sub>	4- <i>i</i> -propyl-Ph	6.53
20						
21	61	A	4-CH <sub>3</sub> -Ph	CH <sub>3</sub>	4-Cl-Ph	5.90
22						
23	62	A	4-C <sub>2</sub> H <sub>5</sub> -Ph	CH <sub>3</sub>	4-Cl-Ph	5.91
24						
25	63	A	4-C <sub>3</sub> H <sub>7</sub> -Ph	CH <sub>3</sub>	4-Cl-Ph	6.23
26						
27	64	A	4- <i>i</i> -propyl-Ph	CH <sub>3</sub>	4-Cl-Ph	6.23
28						
29	65	B	4-Cl-Ph	C <sub>2</sub> H <sub>5</sub>	4-Cl-Ph	5.33
30						
31	66	A	4-F-Ph	C <sub>2</sub> H <sub>5</sub>	4-CH <sub>3</sub> -Ph	6.20
32						
33	67	A	Ph	C <sub>2</sub> H <sub>5</sub>	Ph	5.26
34						
35	68	A	Ph	C <sub>2</sub> H <sub>5</sub>	4-F-Ph	5.58
36						
37	69	A	4-F-Ph	C <sub>2</sub> H <sub>5</sub>	Ph	5.28
38						
39	70	A	2-F-Ph	C <sub>2</sub> H <sub>5</sub>	4-F-Ph	5.30
40						
41	71	A	2-F-Ph	C <sub>2</sub> H <sub>5</sub>	2-F-Ph	5.00

<sup>c</sup>Compound enumeration was assigned on the basis of the original increasing numbering from the oldest to the most recent reference. Table S1 shows the connections between the new and original enumerations.

<sup>a</sup>A = thiomorpholin-4-yl and B = 4-methylpiperazin-1-yl

<sup>b</sup>pMIC = -Log [MIC(μM) x 10<sup>-6</sup>]

**A****B****C**

**Figure 1.** A: monocarbamates (**1a-e**); B: dicarbamates (**2a-f**); C: amides (**3h-i**) of D-4-amino-3-isoxazolidinone placed in the reported pharmacophoric model.<sup>14</sup> HY (hydrophobic feature), RA (aromatic feature), HBA (hydrogen bond acceptor feature). The four pharmacophoric features are color-code according to the original reference.

1  
2  
3  
4  
5  
6 Three of the best mono-probe 3-D QSAR models, A, HD and NA (Table 4 and Figure S1),  
7  
8 accounting for different interaction patterns, were selected for further analysis and the relative 3-D  
9  
10 plots were inspected (Figure 2, Figures S2-S4). A comparison between these plots and the original  
11  
12 pharmacophoric model<sup>14</sup> was performed to check for spatial superposition of plot regions and  
13  
14 pharmacophoric features (compare Figures 2A-2C with Figure 2D). Interpretation of the PLS-  
15  
16 coefficients plots could be helped considering the Equation 1.0 where  $C_n$  is the  $C_{\text{PLS}}$  coefficient in  
17  
18 the  $n$ th grid point,  $X_n$  is the actual field in the  $n$ th grid point,  $Y$  the biological activity and  $n$  the  
19  
20 number of grid points.  
21  
22  
23

$$Y = C_1X_1 + C_2X_2 + \dots + C_nX_n + e.$$

24  
25  
26  
27 Equation 1. General equation for QSARs

28  
29 As addressed by Equation 1,  $C_{\text{PLS}}$  coefficients provide both interpretation of training set data  
30  
31 (explaining the relative influence of each grid point by means of size and sign) and prediction of  
32  
33 test set molecules' biological activity,  $Y$ ; an interaction characterized by a positive (repulsive) field  
34  
35  $X_n$  into a region with positive PLS-coefficient  $C_n$  will produce a positive effect ( $C_n \times X_n$  product is  
36  
37 positive), denoting a positive influence on  $Y$  (higher  $p\text{MIC}$ ); the opposite is valid if the field or the  
38  
39 PLS-coefficient have negative  $X_n$  or  $C_n$ , respectively. A positive effect (still considering  $p\text{MIC}$ s  
40  
41 activities) could be produced as well by a negative (attractive) field  $X_n$  into a region with negative  
42  
43 PLS-coefficient  $C_n$  ( $-C_n \times -X_n$  product is positive) and the opposite effect if the field or the  
44  
45 PLS\_coefficient have positive  $X_n$  or  $C_n$ , respectively.  
46  
47  
48  
49

50  
51 As a result, four areas of the PLS-coefficients plots were distinguished over the N1, C2, C3 and C5  
52  
53 substituents of the pyrrole ring which overlap the pharmacophoric features HY, RA1, HBA and  
54  
55 RA2, respectively, thus suggesting a good agreement between QSAR and pharmacophoric models.  
56

57  
58 All mono-probe 3-D QSAR models clearly suggest that the presence of bulky groups as substituent  
59  
60 at N1, C2, C5 is preferred, especially in N1 and C5 (HY and RA2 features). Moreover, the PLS-  
coefficient plots within thiomorpholines and methylpiperaziny derivatives, (i.e. compounds **60** and

21 in Figure 2) and even more both PLS-coefficients and activity contribution plots (Figures S2-S4) show that at the C3 position steric features are required within certain limits. In particular, concerning the HBA feature, the HD model clearly shows that attractive interactions involving the sulfur of the thiomorpholine group of **60** (the most active compound, Figure S3A), increase the biological activity, while if these are missing or replaced by repulsive interactions, as for **21** (the least active compound), the biological effect decreases (Figure S3B). Therefore, a bulky group like thiomorpholinomethyl, also able to participate in electrostatic interactions, such as hydrogen bonds, is preferred at the C3 position. As for the structural features required for activity, the simultaneous analysis of PLS-loading and score plots were very useful to carry out the most relevant variables from the models (loading plots) and interpret the patterns seen in the score plots. Interesting is the case of the A probe model: starting from the first principal component (PC1), the presence of two clusters, differing each other for their conformational properties, is clearly showed in the scores plot (Figure S5A). As shown in Figure S6 by superimposing the most influencing compounds (absolute higher score values) for each cluster to the PLS-loadings, the most important molecular feature in the PC1 space is related to both different spatial orientations and conformations. Light grey molecules, that are molecules in the positive field cluster (positive PC1), had a higher activity and fill the lower part of the region between the RA2 and HBA features but not between RA1 and HBA. On the contrary, molecules with lower pMICs fill the area between the RA1 and HBA. Therefore a given derivatives able to preferably occupy the region between the RA2 and HBA features, should be endowed of a higher activity than a molecule filling the area between the RA1 and HBA. PC2 and PC3 respectively gave information about substituents at C3 (Figures S5B, S7 and S8), suggesting the presence of bulky groups in the upper areas between the RA2 and HBA and over the HBA features have a detrimental effect on the biological activity.

**Table 3.** CAPP settings

Min Value	Parameter	Max Value	Step
0	PCO	10	1.0
0	Zeroing	0.05	0.005

0 MSDCO 5 1  
 PCO: Positive Cut Off, Zeroing: zeroing of very low data points, MSDCO: Minimum SD Cut Off.

**Table 4.** 3-D QSAutogrid/R PLS models statistical results (CAPP process was applied)

model	P	PC	$r^2$	$q^2_{\text{LOO}}$	$q^2_{\text{K5FCV}}$	$r^2_{\text{YS}}$	$q^2_{\text{YS}}$	V
1	A	3	0.92	0.86	0.85	0.36	-0.33	3758
2	C	3	0.92	0.86	0.85	0.37	-0.33	4492
3	HD	3	0.91	0.85	0.84	0.39	-0.31	1217
4	NA	3	0.91	0.86	0.85	0.31	-0.33	531
5	N	3	0.91	0.85	0.85	0.32	-0.30	477
6	OA	3	0.91	0.85	0.85	0.36	-0.33	658
7	e	4	0.88	0.78	0.76	0.40	-0.48	468
8	d	4	0.91	0.85	0.84	0.35	-0.44	4412

P: Autogrid Probe, PC: optimal number of principal components/latent variables,  $r^2$ : conventional square-correlation coefficient;  $q^2_{\text{LOO}}$ : cross-validation correlation coefficient using the leave-one-out method;  $q^2_{\text{K5FCV}}$ : cross-validation correlation coefficient using the  $k$ -fold cross-validation with 5 random groups and 100 iterations;  $r^2_{\text{YS}}$ : average square-correlation coefficient obtained after Y-scrambling process using 100 iterations;  $q^2_{\text{YS}}$ : average cross-validation correlation coefficient using the leave-one-out method obtained after Y-scrambling process using 100 iterations; V: number of active variables.

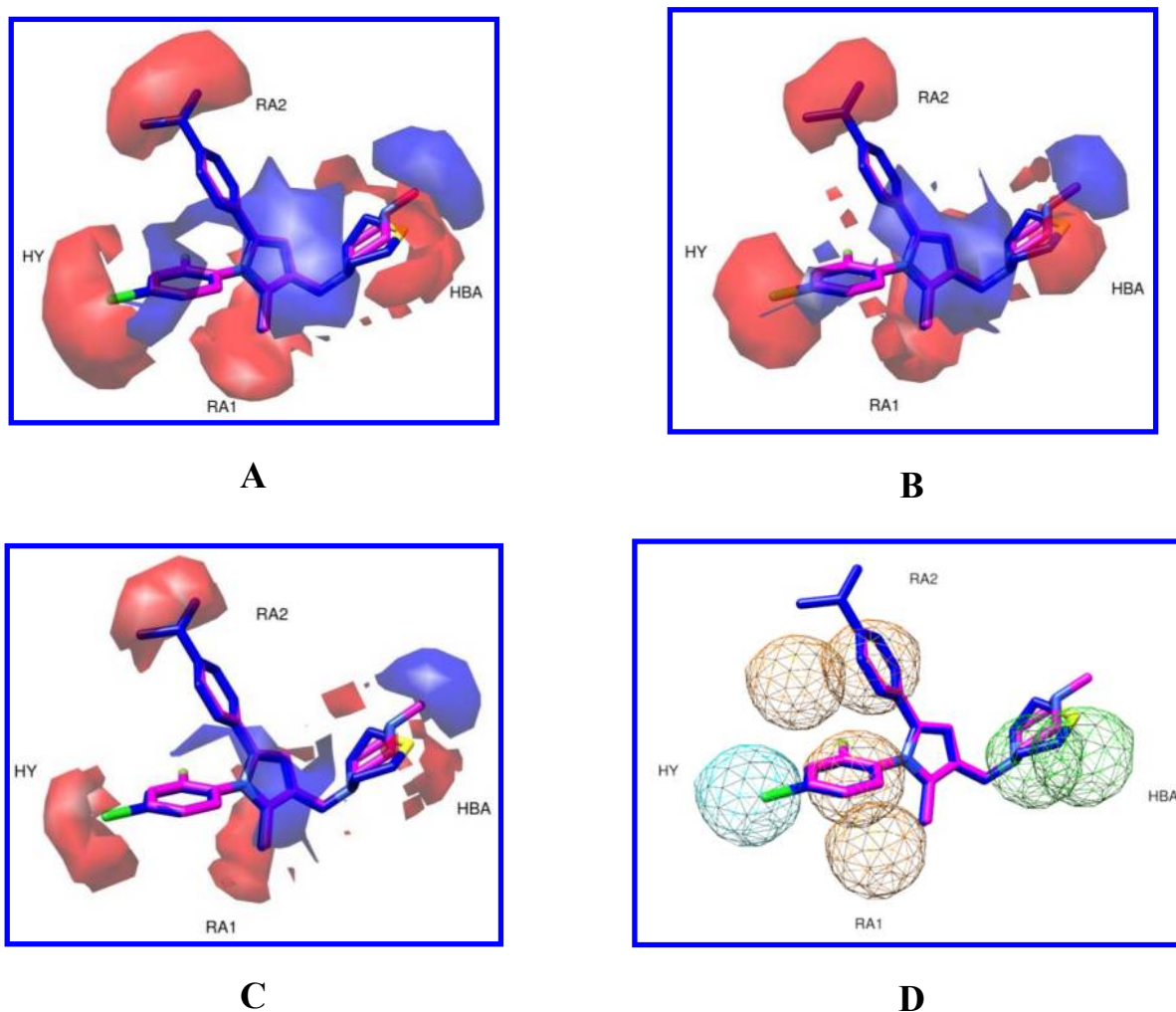


**Figure 2.** The most active (**60** in blue) and the less active (**21** in magenta) compounds are shown. A: PLS-coefficients contour maps derived from A probe analysis (contour levels: 80%; positive: red, negative: blue); B: PLS-coefficients contour maps derived from HD probe analysis (contour levels: 85%; positive: red, negative: blue); C: PLS-coefficients contour maps derived from NA probe analysis (contour levels: 75%; positive: red, negative: blue). D: pharmacophoric features derived from the original pharmacophoric model:<sup>14</sup> HY (hydrophobic feature), RA (aromatic feature), HBA (hydrogen bond acceptor feature).

### *Application of Multi-Probe Guided Region-Variable Selection*

By application of the Multi Probe Guided Region Selection (MPGRS package), as implemented in 3-D QSAutogrid/R,<sup>11</sup> a multi-probe (MP) 3-D QSAR model was derived, representing, the best of our knowledge, the first quantitative pharmacophoric model able to correlate the structural features of pyrrole derivatives with their biological data. The optimal MP 3-D QSAR model was characterized by a  $PC_{FL:SL}=1:3$ ,<sup>11</sup> and as previously reported,<sup>11</sup> its associated statistical coefficients (Table 5, Figure S9) were similar to those of the mono-probe models but the interpretation was greatly enhanced. Applying a  $q^2$  threshold value of 0.4, the most relevant MIFs sub-regions were selected (Figure 3) to build the multi-probe MIF and the resulting MP model condensing in one all the suggestions retrieved by the analysis conducted on the mono-probe models. In particular, the MP PLS-loadings in association with the MP score plots identified the same conformational differences, addressed by the mono-probe models, as the most discriminating aspect in molecular clustering, for example: starting from  $PC_{1:1}$  to  $PC_{1:2}$  a similar clustering in the score plots and in meaning for the descriptors to those in the A mono probe model was noticed (compare Figures S10-S12 and Figures S5-S7), confirming the above assumptions (effect of difference in spatial arrangement and conformation). The MP PLS-coefficient plot showed that the most important regions were spatially and chemically overlapping with the pharmacophoric model<sup>14</sup> (compare Figures 3B and 3D). Taking into account the probe type with the associated PLS-coefficient sign, bulky groups seemed to be required at the N1, C2 and C5 positions (positive coefficients); furthermore negative PLS-coefficients were spread in the proximity of these areas and the fact that chlorine and fluorine substituents are associated to activity enhancement, these additional areas can be related to some electrostatic molecular environment (Figure 3B and 3C) in agreement with the pharmacophoric model.<sup>16, 18</sup> In addition, regarding C3 position (in the lower part of HBA and slightly extended towards RA2) the model indicates that a limited steric repulsion is tolerated and electrostatic endowed groups could be profitable for the activity. Further information about the HBA feature were derived overlapping the clustered molecules (Figure S10B) with both PLS-

loadings and PLS-coefficients at PC<sub>1:3</sub> (Figure 4A and 4B): the implementation of different probes (such as NA and HD) suggested that the presence of bulky groups in the upper areas between the RA2 and HBA and over the HBA feature might have a detrimental effect on the biological activity; i.e. considering the methylpiperazinyl moiety (characterizing most of the negative clustered molecules, Figure 4B2) the methyl group fits the HD areas characterized by a negative PLS-coefficient, while the thiomorpholinomethyl moiety (that discriminate the positive clustered molecules, Figure 4B1) satisfies both steric and electrostatic features leading to higher activities. In this scenario the MP model was able to increase the resolution of the HBA region revealing an extra partial steric role.

**Table 5.** MPGRS. Multi Probe model statistical results

MPGRS 3-D QSAR							
$PC_{FL:SL}$	$r^2$	$q^2_{LOO}$	$q^2_{K5FCV}$	$SDEP_{LOO}$	$SDEP_{K5FCV}$	$r^2_{YS}$	$q^2_{YS}$
1:3	0.88	0.80	0.80	0.32	0.32	0.31	-0.31

$PC_{FL:SL}$ : optimal number of principal first level (FL) and second level (SL) components for the MPGRS model;  $r^2$ : conventional square-correlation coefficient;  $q^2_{LOO}$ : cross-validation correlation coefficient using the leave-one-out method;  $q^2_{K5FCV}$ : cross-validation correlation coefficient using the  $k$ -fold cross-validation with 5 random groups and 100 iterations.

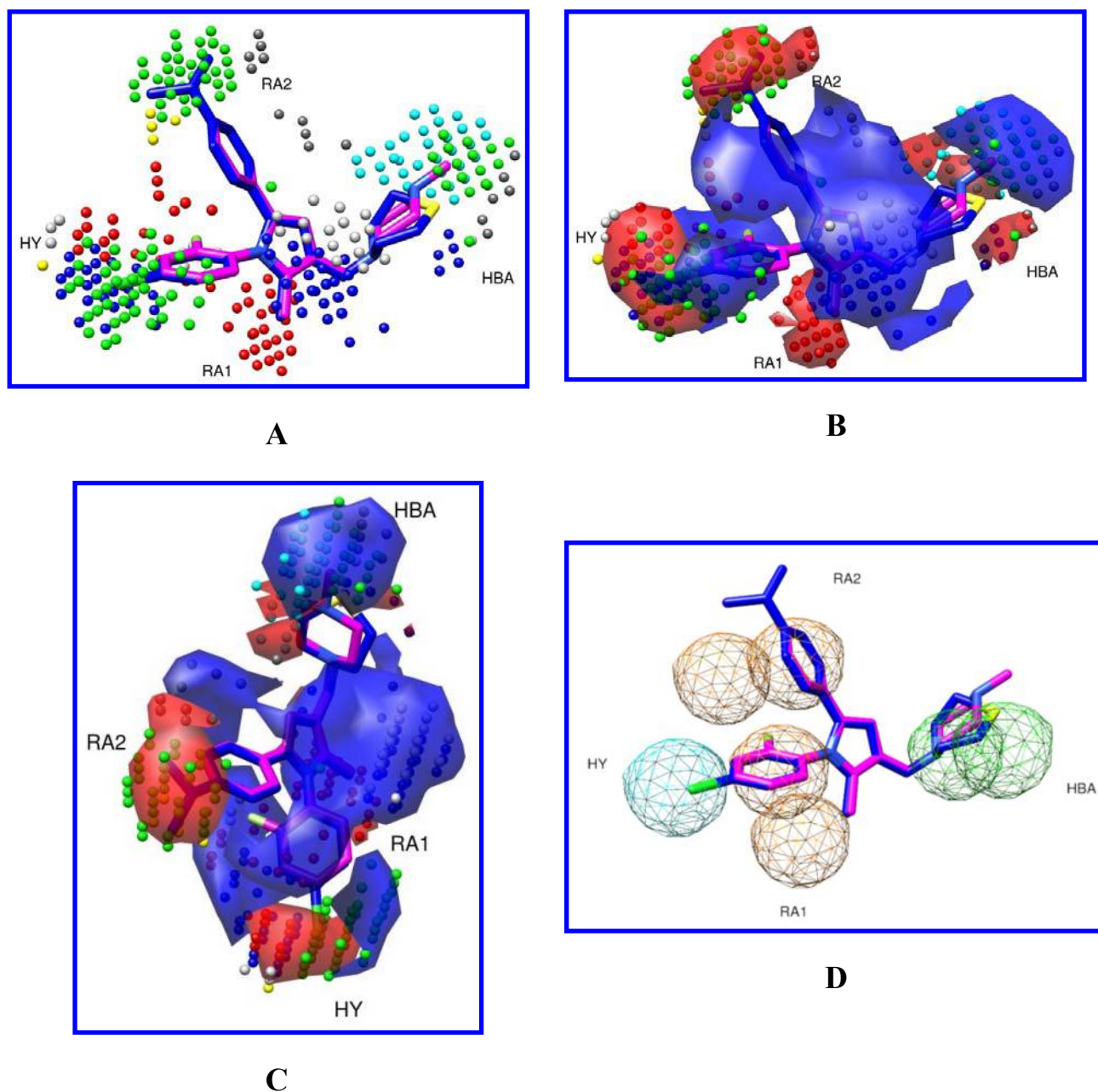


**Figure 3.** MPGRS. A: key points: the points are color coded according to that reported in Table S5; B: key points with PLS-coefficients contour maps (contour levels: positive 85%, red; negative 95%, blue); C: top view, key points with PLS-coefficients solid contour maps (contour levels: positive 85%, red; negative 95%, blue). The most active (**60** in blue) and the less active (**21** in magenta) compounds are shown. D: pharmacophoric features derived from the original pharmacophoric model:<sup>14</sup> HY (hydrophobic feature); RA (aromatic feature), HBA (hydrogen bond acceptor feature).

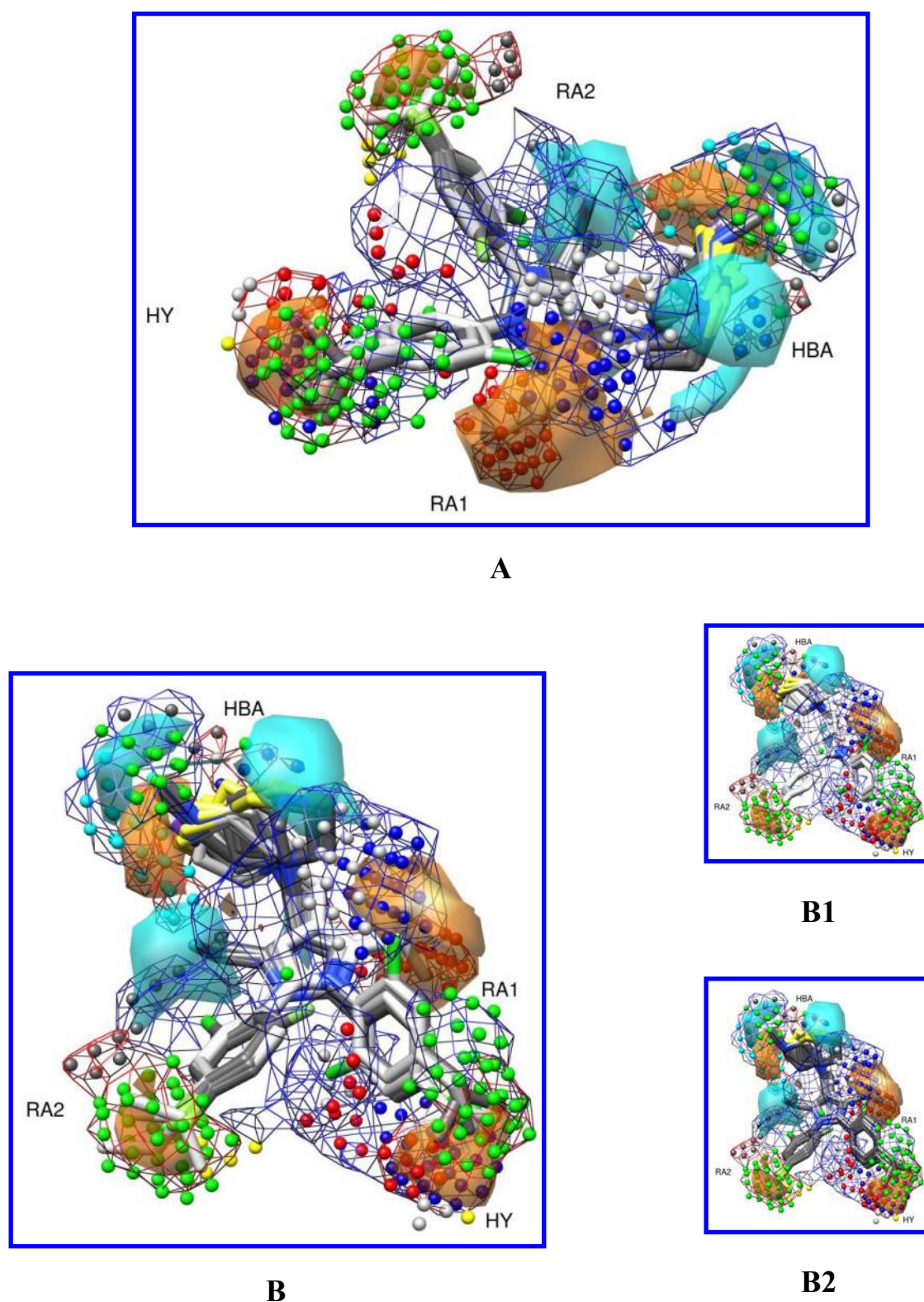


**Figure 4.** MPGRS. PLS-loadings contour maps at  $PC_{1:3}$  (contour levels: 75%; positive: orange, negative: cyan) with PLS-coefficients (mesh levels: positive 85%, red; negative 95%, blue) and key points (see Table S5 for color coding). The ten most important molecules for each cluster are plotted and color coded (compounds in the positive loading field in light gray; compounds in the negative loading field in dark grey). A: side view; B: frontal view; B1: frontal view of only positive clustered molecules; B2: frontal view of only negative clustered molecules. HY (hydrophobic feature), RA (aromatic feature), HBA (hydrogen bond acceptor feature).

### *External Test Set Prediction Analysis.*

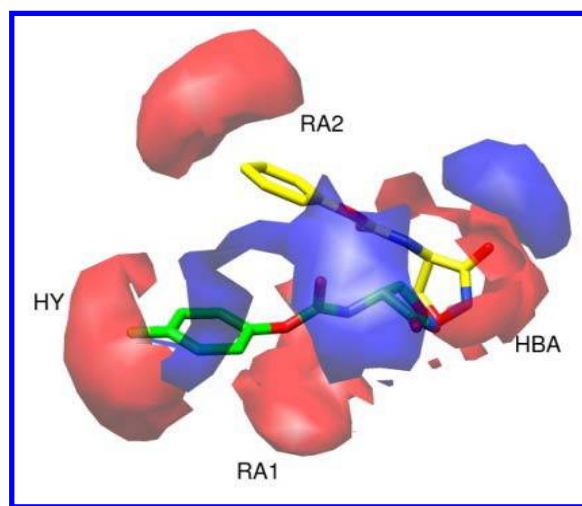
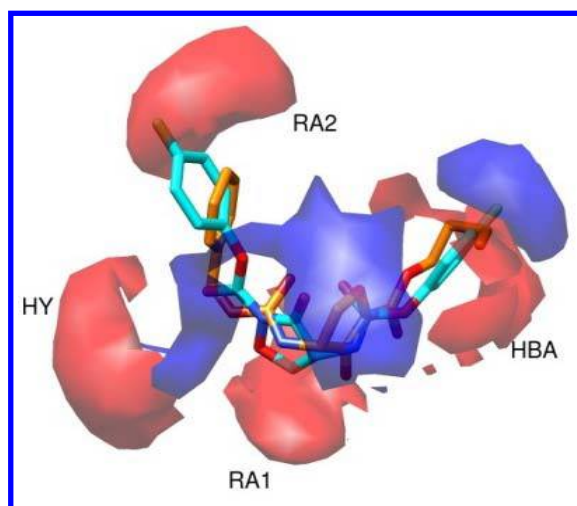
The eight 3-D QSAutogrid/R mono probe models were externally validated using the 13 newly synthesized monocarbamates (**1a-e**), dicarbamates (**2a-f**) and amides (**3h-i**) (Table 1). A fact must be emphasized: since the training set was composed only by pyrrole derivatives to directly compare the quantitative models with the original pharmacophoric assumptions, the resulting quantitative structure-activity relationships were based, mostly, on the characteristics of the scaffolds composing the training set. This may result in a limitation of the models to predict the activities of other molecular classes: in this case, specifically, a major difference between the two sets, training set and test set, was represented by the fact that the former was characterized by the pyrrole ring, which permits a quadruple branching able to satisfy simultaneously the different pharmacophoric areas; on the contrary, the compounds of the test set were characterized by a double branching. Despite this fact, and considering also that the test set molecules showed similar activity values (total pMIC activity range = 1.31 log unit), acceptable errors of prediction (SDEP coefficients all below the unit except for the d model) were obtained (Table 6); but an analysis focused only on the statistical SDEP values or experimental *vs* predicted plots (Figure S13) could be misleading. In fact, analyzing only the statistical results might seem that the PLS models had good predictive ability towards the isoxazolidinone derivatives, while considering only the experimental *vs* predicted plots the same conclusion could not be reached. In this case it was helpful to analyze both of these information, together with the average absolute error of predictions (AAEP, Table S6), for each molecule from all the 3-D QSAR mono probe models and finally their placement in the 3-D space of PLS-coefficients. Analyzing, for each test set molecule, the AAEP from all the eight mono probe models stood out the good predictive capacity toward 10 of these, while for **1a**, **2c** and **2e** the AAEPs were 1.05, 1.50 and 1.72 respectively. These compounds were over-predicted and this can be sought precisely in the dependence of the model from the training set congenerousness and from consequent inevitable alignment limitations. Furthermore **1a** was predicted more active than **1d** likely due to the fact that its isoxazolidinonic carbonyl group was perfectly superimposed to the

1  
2  
3 training set most active compound (**60**) thiomorpholinic sulfur atom, showing how important was  
4  
5 for the models the presence of a group capable to accept hydrogen bonds in the HBA space. It  
6  
7 should be stressed, however, that such molecules (**1a**, **2c** and **2e**), probably, would have been  
8  
9 discarded by adopting the original pharmacophoric model,<sup>14</sup> in fact: compound **1a** misses the RA1  
10  
11 and HY features while RA2 and HBA are satisfied with the presence of a phenyl in R1 and carbonyl  
12  
13 group of the isoxazolidinone ring respectively; **2c** satisfies only the RA2 feature, and partially the  
14  
15 HBA feature with the presence of the *p*-methoxyphenylic oxygen; **2e** accomplishes the HY and  
16  
17 partially the RA1 feature; whereas all the 3-D QSAR models are able to frame their level of  
18  
19 activity: for this reason and for the above considerations, the models show a good predictive ability  
20  
21 although different scaffold endowed molecules were used as test set. As examples of the 3-D QSAR  
22  
23 model application the most and least active monocarbamate derivatives (**1d** and **1a**, respectively)  
24  
25 overlapped with the A probe model PLS-coefficients are depicted in Figure 5A, while the most and  
26  
27 the least active dicarbamate molecules (**2d** and **2f**, respectively) are reported in Figure 5B. Despite  
28  
29 the above considerations differences in experimental activities appears to be determined by a better  
30  
31 overlap of the aromatic ring with the *p*-fluorine on the HY and RA2 regions  
32  
33  
34  
35  
36  
37  
38  
39  
40

41 **Table 6.** Test Set predictions

P	PC	SDEP <sub>EXT</sub>
A	3	0.88
C	3	0.88
HD	3	0.81
NA	3	0.82
N	3	0.83
OA	3	0.84
e	4	0.90
d	4	1.51

42 SDEP values considering the optimal PCs; P: AutoGrid Probe; PC: optimal  
43 number of principal components/latent variables; SDEP<sub>EXT</sub>: standard deviation  
44 error of prediction (or root mean squared error of prediction, RMSEP) for the  
45 external test set.  
46  
47  
48  
49  
50  
51  
52  
53  
54  
55  
56  
57  
58  
59  
60

**A****B**

**Figure 5.** PLS-coefficients contour maps. A: AutoGrid/R PLS-coefficients contour maps derived from the A probe analysis (contour levels: 80%; positive: red, negative: blue; **1a**: yellow; **1d**: green); B: AutoGrid/R PLS-coefficients contour maps derived from the A probe analysis (contour levels: 80%; positive: red, negative: blue; **2d**: cyan; **2f**: orange). HY (hydrophobic feature), RA (aromatic feature), HBA (hydrogen bond acceptor feature).

Analogously, the MP model predictions were in good agreement with those of the mono probe models (Table 7). The 3-D QSAR MP plots showing the most active and less monocarbamates and dicarbamates derivatives (Figure 6) indicated the lack of a simultaneous coverage of the different regions addressed by the PLS-coefficients. However, as shown in Figure 6 was confirmed the importance of hydrophobic substituents in the HY and RA2 areas, which should determine the highest activities of **1d** and **2d**.

**Table 7.** MPGRS. Multi Probe model Test Set predictions

P	PC <sub>FL:SL</sub>	SDEP <sub>EXT</sub>
AutoGrid MP	1:3	0.89

SDEP values considering the optimal first level and second level PCs. P:AutoGrid Multi-Probe; PC<sub>FL:SL</sub>: optimal first level and second level PC; SDEP<sub>EXT</sub>: standard deviation error of prediction (or root mean squared error of prediction, RMSEP) for the external test set.

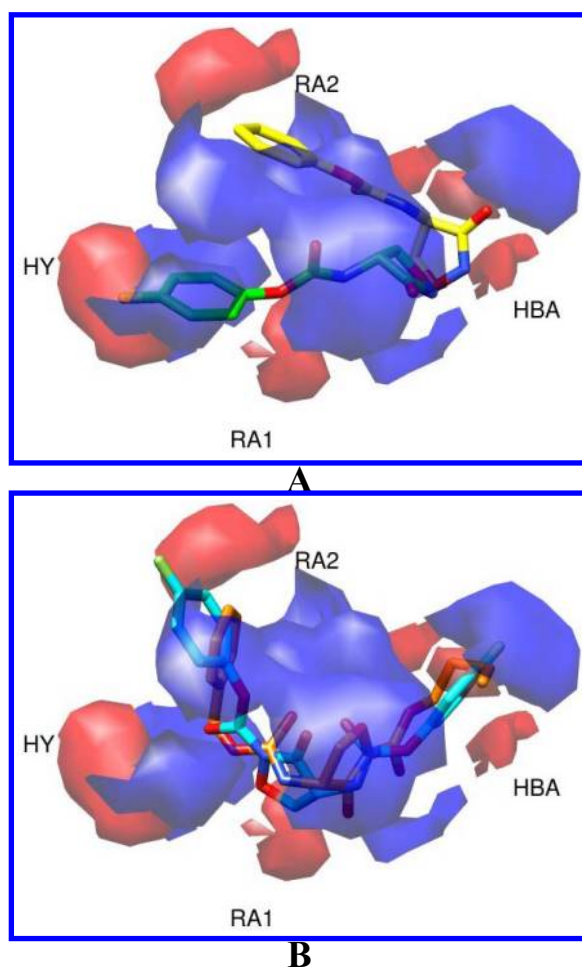
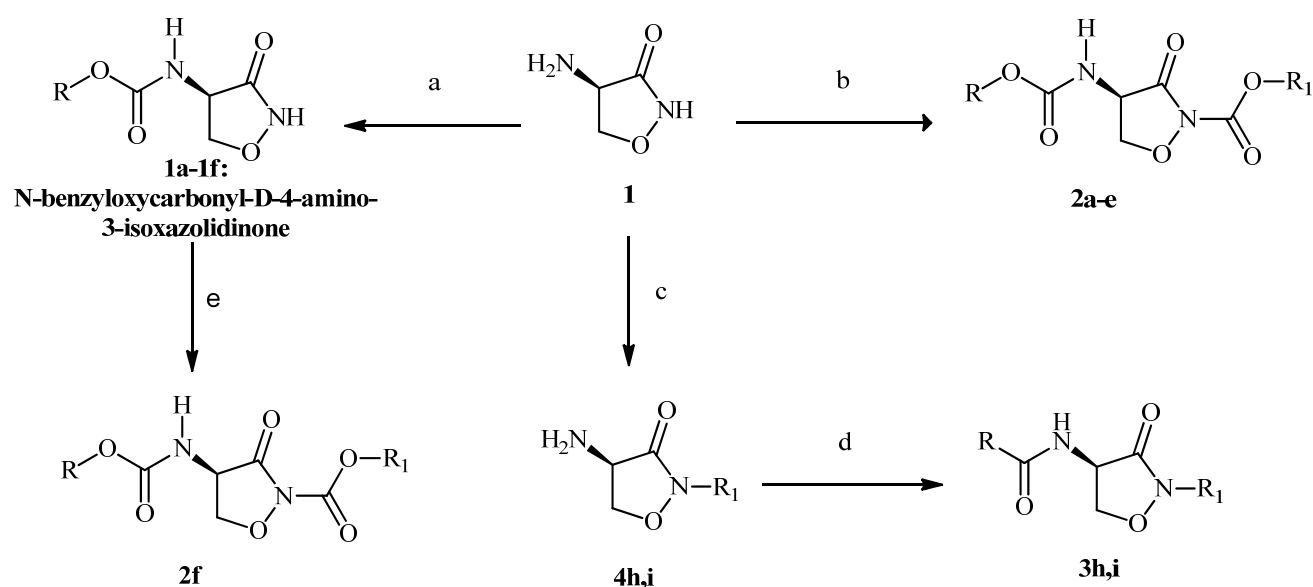


**Figure 6.** MPGRS. A: PLS-coefficients contour maps at PC<sub>1:3</sub> (contour levels: positive 85%, red; negative 95%, blue; **1a**: yellow; **1d**: green); B: PLS-coefficients contour maps at PC<sub>1:3</sub> (contour levels: positive 85%, red; negative 95%, blue; **2d**: cyan; **2f**: orange). HY (hydrophobic feature), RA (aromatic feature), HBA (hydrogen bond acceptor feature).

## 2.2 Chemistry

The synthesis of compounds (**1a-e**) and (**2a-f**) was carried out modifying a literature procedure described by Stammer and coworkers,<sup>20</sup> by treatment of , D-4-amino-3-isoxazolidinone in weakly alkaline media (1M NaHCO<sub>3</sub>) with the corresponding chloroformate to obtain both mono- and dicarbamate derivatives, as illustrated in Scheme 1.



**Scheme 1.** a) R-O-CO-Cl, 1M NaHCO<sub>3</sub>, 0°C 3h, 4M HCl; b) R-O-CO-Cl, NaHCO<sub>3</sub>, 0°C, 15h; c) 0.1 M TEAHFP in CH<sub>3</sub>CN, 30 mAcm<sup>-2</sup>, D-4-amino-3-isoxazolidinone 1 eq (15 min), R<sub>1</sub>-Br; d) 3-CF<sub>3</sub>-C<sub>6</sub>H<sub>4</sub>COCl, TEA, CHCl<sub>3</sub>; e) **1f**, n-Bu-O-CO-Cl, 1M NaHCO<sub>3</sub>, 0°C, 24h.

The derivatives **1a-f** were prepared by regioselective acylation of the 4-amino group using the appropriate chloroformates at low temperature for short reaction time (0 °C for 3 h); then pure solids **1a-f** were obtained by acidification with 4M HCl. Dicarbamate derivatives **2a-e** were

1  
2  
3 synthesized dissolving the D-4-amino-3-isoxazolidinone in a basic solution at 0°C and the selected  
4 chloroformates were dropwise added. **2a-e** gradually precipitate in 12 h from the aqueous solution.  
5  
6  
7 The compound **2f** was obtained by treatment of **1f** with n-butylchloroformate in alkaline solution.  
8  
9  
10 N-2-(alkyl)-4-amino-3-oxoisoxazolidinone -**4h-i** were synthesized by an electrochemical reaction as  
11  
12 previously reported.<sup>21</sup> Then crude **4h-i** were acylated with 3-trifluoromethyl benzoyl chloride in  
13  
14 chloroform / TEA to give the amide derivatives **3h-i**.  
15  
16

17 In order to verify the racemization of the  $\alpha$  carbon of D-4-amino-3-isoxazolidinone in the reaction  
18  
19 conditions, we have analyzed by chiral HPLC the enantiopurity of (*R*)-**3h** and (*S*)-**3h**, obtained with  
20  
21 the same synthetic procedure starting from (*R*)-4-amino-3-isoxazolidinone and (*S*)-4-amino-3-  
22  
23 isoxazolidinone. Chiralpak Column IC 250 mm x 4.6 mm I.D was used with *n*-hexane-2-propanol  
24  
25 75/25 (v/v) as eluent at flow rate of 1.0 mL/min at the temperature of 25°C. In both the  
26  
27 chromatogram of (*R*)-**3h** and (*S*)-**3h** an enantiomeric excess > 99.0 % was observed (Figure S15).  
28  
29  
30  
31  
32  
33

### 34 **2.3 Biological Activity of Synthesized Compounds**

35  
36 The compounds were assayed for their antimycobacteria activity toward *M. tuberculosis* H37Rv  
37  
38 (ATCC 27294). The minimal concentration inhibiting visible growth of mycobacteria was  
39  
40 determined for each compounds.  
41  
42

43 Concerning the data reported in Table 7 only the acylation of 4-amino group and acylation or  
44  
45 alkylation of N-2 of D-4-amino-3-isoxazolidinone influenced the antitubercular activity leading to  
46  
47 a MIC value of 3.1  $\mu\text{g/mL}$  (as in the case of **1d** and **2d**). Most of the tested compounds showed the  
48  
49 same activity of the 4-amino-3-isoxazolidinone (32  $\mu\text{g/mL}$ ), while **1d** and **2d** resulted more active  
50  
51 (3.1  $\mu\text{g/mL}$ ) and only the compound **3h** resulted the less active (64  $\mu\text{g/mL}$ ).  
52  
53  
54  
55  
56  
57  
58  
59  
60

**Table 7.** MIC data for D-4-amino-3-isoxazolidinone derivatives

compd	MIC( $\mu\text{g/mL}$ ) <sup>a</sup>	pMIC <sup>b</sup>
<b>1a</b>	32	3.84
<b>1b</b>	32	3.87
<b>1c</b>	32	3.90
<b>1d</b>	3.1	4.89
<b>1e</b>	32	3.97
<b>2a</b>	32	4.03
<b>2b</b>	32	4.06
<b>2c</b>	32	4.10
<b>2d</b>	3.1	5.09
<b>2e</b>	32	4.11
<b>2f</b>	32	4.02
<b>3h</b>	64	3.78
<b>3i</b>	32	4.13

<sup>a</sup>*M. tuberculosis* H37Rv (ATCC 27294) was used; MIC values represent the minimal concentrations of compounds completely inhibiting visible growth of mycobacteria.

<sup>b</sup>pMIC = -Log [MIC( $\mu\text{M}$ ) x 10<sup>-6</sup>]

### 3. Conclusion

In this paper we present the first application of a quantitative pharmacophoric model able to define and correlate the needed chemical characteristics with antitubercular activity of a previously reported class of antimycobacterial agents.<sup>8,13-17</sup> Eight 3-D QSAR mono probe models and a multi probe (MP) model were built showing appreciable statistical coefficients, and allowing an accurate definition of the structure-activity relationships on the basis of pyrrole derivatives used as training set. The MP 3-D QSAR model let to define the training set molecular features and their three-dimensional positioning, configuring itself as a quantitative pharmacophoric model. Furthermore it was possible to elucidate the effect of conformational differences on the biological activity. As a further assessment the multi probe information was compared with the original pharmacophoric model, previously developed by us,<sup>14</sup> showing an high degree of correspondence.

Independently, a series of 13 isoxazolidinone derivatives **1-3** (Table 1) was synthesized and tested as new antitubercular compounds. The new compounds showed MIC values in the micromolar range. In particular among the monocarbamates and dicarbamates, derivatives **1d** and **2d** showed the higher biological activities. Although there are limitations due to structural differences between the

1  
2  
3 molecules of the training set and those of derivatives **1-3**, the latter were used as an external test set  
4  
5 to evaluate the models' predictive capabilities. All the 3-D QSAR models showed prediction errors  
6  
7 (Tables 6 and 7), against these structurally unrelated molecules, with an acceptable degree of  
8  
9 approximation.

10  
11  
12 The application of the models allowed to clarify the role of halogens and phenyl rings in **1a-e** and  
13  
14 **2a-f**. Considering all these outcomes, the MP 3-D QSAR model could represent a useful tool for the  
15  
16 design of new antitubercular drugs.  
17  
18  
19  
20  
21

## 22 **4. Experimental Section**

### 23 4.1 Molecular Modeling and 3-D QSAR

24  
25 All calculations used a 6 blades (8 Intel-Xeon E5520 2.27 GHz CPU and 24 GB DDR3 RAM each)  
26  
27 cluster (48 CPU total) running Debian GNU/Linux 6.0 64 bit operating system. A series of 71  
28  
29 previously described pyrrole derivatives<sup>10, 15, 19</sup> were used to build 8 single probe and a multi probe  
30  
31 3-D QSAR models using the 3-D QSAutogrid/R procedure.<sup>11</sup> The obtained models were tested  
32  
33 predicting the activities of the monocarbamates (**1a-e**), dicarbamates (**2a-f**) and amides (**3h,i**) of D-  
34  
35 4-amino-3-isoxazolidinone derivatives.  
36  
37  
38  
39  
40  
41  
42

#### 43 *Training set selection:*

44  
45 Starting from a training set composed by 90 pyrrole derivatives,<sup>10, 15, 19</sup> a selection based on inner  
46  
47 relationship analysis were conducted to improve the robustness and prediction capabilities of the 3-  
48  
49 D QSAR models: this leads to a final training set composed by 71 molecules (Table 2).  
50  
51  
52  
53  
54

#### 55 *Alignment rules:*

56  
57 Training Set: Training set compounds were first submitted to a conformational search following a  
58  
59 computational protocol previously described.<sup>10</sup> Next, each compound with its conformational  
60  
models was aligned to the pharmacophoric model with the flexible fitting method implemented in

1  
2  
3 Discovery Studio (version 3.0, Accelrys, Inc., San Diego, CA), that allows slight modification of  
4  
5 each conformation to better fit the pharmacophore.  
6  
7

8 Test Set: The new 13 derivatives were aligned using the Surflex-Sim<sup>22</sup> software which has been  
9  
10 chosen since it's a valuable tool in ligand-based drug discovery, free for academics, and its  
11  
12 alignment process is based on morphological similarities. The query molecules' poses were  
13  
14 optimized to the compounds used as training set to maximize 3D similarity.  
15  
16

17 As shown in Figures S16, S17, Tables S9 and S10, similar results were obtained using the same  
18  
19 alignment software (pharmacophoric alignment) adopted for the training set. The choice of Surflex  
20  
21 alignment was not dictated by the improvement (although negligible respect the pharmacophoric  
22  
23 one) in prediction, but by the fact that, in our view, this is a further confirmation of the robustness  
24  
25 of the models, always taking into account the above limits. Indeed, using two different procedures  
26  
27 of alignment, results are comparable and this should show that the predictive capability of the  
28  
29 models is stable and in the specific case scarcely influenced. Further clarifications on the  
30  
31 differences in prediction (as in the case of **1d** and **2d**) would be only speculative since the presence  
32  
33 of similar activity values with a limited total pMIC activity range.  
34  
35  
36  
37

38 Strategies for different alignments were also tried leading to not consistent prediction supporting  
39  
40 that the best alignment/prediction is that above reported.  
41  
42  
43  
44

#### 45 *Molecular Interaction Fields Calculation.*

46  
47 As reported,<sup>11</sup> MIFs were generated using the AutoGrid Software (AutoDock Suite,<sup>23</sup> based on the  
48  
49 AMBER united-atom Force Field) implemented in the 3-D QSAutogrid/R procedure, considering 8  
50  
51 different probes. Interaction energies between the selected probes and each molecule were  
52  
53 computed using a grid spacing of 1 Å (Tables S8). The xyz coordinates (in angstroms) of the grid  
54  
55 rectangular box used for the computation were Xmin/Xmax = -9.828/12.172, Ymin/Ymax = -  
56  
57 9.021/8.979, Zmin/Zmax = -10.481/9.519.  
58  
59  
60

### *Statistical Analysis.*

Through the D2M package<sup>11</sup> 8 3-D QSAR PLS models were built. During the model definition the assessment of quality and robustness was conducted via two cross-validation (CV package)<sup>11</sup> procedures as follows: (1) Leave-One-Out (LOO) and (2) k-Fold (KF, 5-random groups and 100 iterations) methodologies. Initially, the raw models (Tables S2) were optimized through the Combinatorial Analysis of Pretreatment Parameters (CAPP package)<sup>11</sup> setting the pretreatment intervals as listed in Table 3, using the k-fold cross-validation with 5-random groups and 100 iterations and monitoring the  $q^2$  and SDEP values. A total of 726 combinations, for each 3-D QSAR model, were processed using 5% sPRESS reduction<sup>11</sup> to select the optimal pretreatment combination and derive the pretreated PLS models; this led to an average  $q^2$  K5FCV value increment equal to 14% (Tables S4). Furthermore the scrambling approach, Y-Scrambling, (package YS)<sup>11</sup> was applied to investigate the presence of chance correlations using 100 iterations. Considering the obtained good overall statistical coefficients together with the absence of chance correlations (Table 4, TableS3 and Figure S1), no further variable selection steps were performed. By the application of the MPGRS package,<sup>11</sup> a MP 3-D QSAR PLS model was then derived by selecting the most informative subregions for each of the eight considered probe; the same CV and scrambling procedures as those of the mono probe models were performed and the optimal MP 3-D QSAR model was selected according to the  $q^2_{FL:SL}$  values.<sup>11</sup> Similar statistical coefficients to those of the mono probe models were obtained (Table 5, Figure S9) and no further variable selection were performed; finally the most relevant MIFs subregions were selected applying a  $q^2$  threshold value of 0.4.

## **4.2 Chemistry**

D-4-amino-3-isoxazolidinone and all chloroformates were purchased from Sigma-Aldrich (Milano, Italy). All other reagents and solvents were of higher analytical grade. N-benzyloxycarbonyl-D-4-amino-3-isoxazolidinone (**1f**) was prepared according to Stammer et al..<sup>20</sup> Melting points were

1  
2  
3 determined on Tottoli apparatus (Buchi) and are uncorrected. Vibrational spectra were recorded on  
4  
5 a Spectrum One ATR Perkin Elmer FT-IR spectrometer.  $^1\text{H}$  and  $^{13}\text{C}$ -NMR spectra were acquired on  
6  
7 a Bruker AVANCE-400 spectrometer at 9.4 Tesla, in DMSO- $d_6$  or  $\text{CDCl}_3$  at 27°C; chemical shift  
8  
9 values are given in  $\delta$  (ppm) relatively to TMS as internal reference, coupling constants are given in  
10  
11 Hz.  
12

13  
14  
15 Mass spectra were recorded on: a API-TOF Mariner by Perspective Biosystem (Straford, Texas,  
16  
17 USA), samples were injected by an Harvard pump using a flow rate of 5-10  $\mu\text{l}/\text{min}$ , infused in the  
18  
19 Electrospray system; a TSQ quadrupole Mass spectrometer by Thermofinnigan (S. Jose, California,  
20  
21 USA) operating in  $\text{CH}_4$  / CI conditions, samples were introduced in the CI source by a direct  
22  
23 insertion probe. Elemental analyses were obtained by a PE 2400 (Perkin-Elmer) analyzer.  
24  
25  
26  
27  
28

### 29 30 *General procedure for synthesis of monocarbamates 1a-e*

31  
32 Compounds **1a-e** were prepared by a modified procedure described by Stammer *et al.*,<sup>20</sup>: briefly, to  
33  
34 0.5 mmol of D-4-amino-3-isoxazolidinone, dissolved in 1.2 mL of aqueous 1M  $\text{NaHCO}_3$ , cooled in  
35  
36 an ice bath, 1.0 mmol of the corresponding chloroformate was added and the solution stirred for 3  
37  
38 hours at 0°C. Little amounts of precipitate that could be formed were filtered off and the solution,  
39  
40 kept to 0°C, was acidified to pH 4 with 4M aqueous HCl. After 30 min, the white fine precipitate  
41  
42 was collected by centrifugation and washed with cold water. The collected carbamates **1a-e** were  
43  
44  
45 crystallized from water.  
46  
47  
48  
49  
50

### 51 *Synthesis of (R)-phenyl-(3-oxoisoxazolidin-4-yl)carbamate (1a)*

52  
53 **1a** Was obtained as white crystalline solid in 75% yield, mp 148- 9°C.  $^1\text{H}$  NMR (DMSO- $d_6$ ): 11.52  
54  
55 (1H, bs,  $\text{D}_2\text{O}$  exchange); 8.37 ( 1H, s,  $\text{D}_2\text{O}$  exchange); 7.38 ( t, 2H, J = 8.56 Hz); 7.21 ( t, 1H, J =  
56  
57 7.58 Hz); 7.12 ( d, 2H, J = 8.56 Hz); 4.65-4.60, ( m, 1H); 4.56 ( t, 1H, J = 9.78 Hz); 4.03 (t, 1H, J =  
58  
59 8.32 Hz).  $^{13}\text{C}$  NMR (DMSO- $d_6$ ): 170.5; 154.9; 151.4; 129.9; 125.9; 122.3; 72.2; 53.5. FT-IR ( $\text{cm}^{-1}$ ):  
60  
3339, 1709, 1655. MS/ESI:  $(\text{M}+\text{H})^+$  223.0730 (m/z).

1  
2  
3  
4  
5  
6 *Synthesis of (R)-4-methylphenyl-(3-oxoisoxazolidin-4-yl)carbamate (1b)*  
7

8 **1b** Was obtained as white crystalline solid in 75% yield, mp 195-6°C. <sup>1</sup>H NMR (DMSO-*d*<sub>6</sub>): 11.54  
9 (bs, 1H, D<sub>2</sub>O exchange); 8.30 (s, 1H, D<sub>2</sub>O exchange); 7.16 (d, 2H, J = 8.56 Hz); 6.99 (d, 2H, J =  
10 8.56 Hz); 4.66-4.59 (m, 1H); 4.55 (t, 1H, J = 10.35 Hz); 4.02 (t, 1H, J = 8.32 Hz); 2.28 (s, 3H). <sup>13</sup>C  
11 NMR (DMSO-*d*<sub>6</sub>): 169.9; 154.4; 148.5; 134.2; 129.6; 121.3; 71.6; 52.8; 20.3. FT-IR (cm<sup>-1</sup>): 3305,  
12 1709, 1654. MS/ESI: (M+H)<sup>+</sup> 237.0874 (m/z).  
13  
14  
15  
16  
17  
18  
19

20  
21  
22 *Synthesis of (R)-4-methoxyphenyl-(3-oxoisoxazolidin-4-yl)carbamate (1c)*  
23

24 **1c** Was obtained as white crystalline solid in 70% yield, mp 155-6°C. <sup>1</sup>H NMR (DMSO-*d*<sub>6</sub>): 11.45  
25 (bs, 1H, D<sub>2</sub>O exchange); 8.27 (s, 1H, D<sub>2</sub>O exchange); 7.02 (d, 2H, J = 9.06 Hz); 6.91 (d, 2H, J =  
26 9.06 Hz); 4.64-4.59 (m, 1H); 4.54 (t, 1H, J = 9.29 Hz); 4.02 (t, 1H, J = 9.29 Hz); 3.73 (s, 3H). <sup>13</sup>C  
27 NMR (DMSO-*d*<sub>6</sub>): 170.0; 156.5; 154.6; 144.2; 122.5; 114.2; 71.6; 55.4; 52.8. FT-IR (cm<sup>-1</sup>): 3314,  
28 1709, 1655. MS/ESI: (M+H)<sup>+</sup> 253.0790 (m/z).  
29  
30  
31  
32  
33  
34  
35  
36  
37

38 *Synthesis of (R)-4-fluorophenyl-(3-oxoisoxazolidin-4-yl)carbamate (1d)*  
39

40 **1d** Was obtained as white crystalline solid in 70% yield, mp 175-6°C. <sup>1</sup>H NMR (DMSO-*d*<sub>6</sub>): 11.54  
41 (bs, 1H, D<sub>2</sub>O exchange); 8.39 (s, 1H, D<sub>2</sub>O exchange); 7.16 (d, 2H, J = 8.56 Hz); 6.98 (d, 2H, J = 8.56  
42 Hz); 4.68-4.63 (m, 1H); 4.55 (t, 1H, J = 9.56 Hz); 4.03 (t, 1H, J = 8.80 Hz). NMR (DMSO-*d*<sub>6</sub>):  
43 155.9 (d, J = 237.8 Hz); 154.1; 147.3; 123.9 (d, J = 7.32 Hz); 116.5; 116.0 (d, J = 22.7 Hz); 72.0;  
44 53.4. FT-IR (cm<sup>-1</sup>): 3320, 1712, 1699. MS/CI: (M+H)<sup>+</sup> 241 (m/z).  
45  
46  
47  
48  
49  
50  
51  
52  
53

54 *Synthesis of (R)-4-bromophenyl-(3-oxoisoxazolidin-4-yl)carbamate (1e)*  
55

56 **1e** Was obtained as white crystalline solid in 75% yield, mp 180-1°C. <sup>1</sup>H NMR (DMSO-*d*<sub>6</sub>): 11.55  
57 (bs, 1H, D<sub>2</sub>O exchange); 8.42 (s, 1H, D<sub>2</sub>O exchange); 7.22 (d, 2H, J = 8.56 Hz); 7.16 (d, 2H, J =  
58 8.56 Hz); 4.69- 4.62 (m, 1H); 4.56 (t, 1H, J = 9.88 Hz); 4.04 (t, 1H, J = 8.80 Hz). <sup>13</sup>C NMR (DMSO-  
59  
60

1  
2  
3  $d_6$ ): 170.0; 156.5; 154.6; 144.2; 122.5; 114.2; 71.6; 52.8. FT-IR ( $\text{cm}^{-1}$ ): 3330, 1715, 1705. MS/CI:  
4  
5  
6  $(\text{M}+\text{H})^+$  302 (m/z).

7  
8 *General procedure for synthesis of dicarbamates 2a-f*

9  
10 50 mg (0.5 mmol) of D-4-amino-3-isoxazolidinone were dissolved in 1.2 mL of aqueous 1M  
11  
12  $\text{NaHCO}_3$  and cooled at  $0^\circ\text{C}$  and 1.0 mmol of the corresponding chloroformate was added and the  
13  
14 solution was stirred for 15 h. The obtained precipitates were collected by centrifugation, washed  
15  
16 three times with 2 mL of water and dried under reduced pressure to give compounds **2a-f**  
17  
18 subsequently crystallized from benzene.  
19  
20  
21

22  
23  
24 *Synthesis of (R)-phenyl-3-oxo-4-[(phenoxycarbonyl)amino]isoxazolidine-2-carboxylate (2a)*

25  
26  
27 **2a** Was obtained as white crystalline solid in 85 % yield, mp 159-60.  $^1\text{H}$  NMR ( $\text{DMSO}-d_6$ ): 8.58  
28  
29 (bs, 1H,  $\text{D}_2\text{O}$  exchange); 7.47 (t, 2H,  $J = 7.83$  Hz); 7.41 (t, 2H,  $J = 7.58$  Hz); 7.33 (t, 1H,  $J = 6.48$   
30  
31 Hz); 7.24 (d, 2H,  $J = 7.83$  Hz); 7.23 (d, 1H,  $J = 6.70$  Hz); 7.16 (d, 2H,  $J = 7.58$  Hz); 5.03- 4.97 (  
32  
33 m, 1H); 4.80 (t, 1H,  $J = 10.15$  Hz); 4.31 (t, 1H,  $J = 8.68$  Hz).  $^{13}\text{C}$  NMR ( $\text{DMSO}-d_6$ ): 166.4; 154.1;  
34  
35 150.6; 149.5; 145.7; 129.8; 129.4; 126.6; 125.4; 121.6; 121.4; 69.8; 53.0. FT-IR ( $\text{cm}^{-1}$ ): 3344,  
36  
37 1789, 1736, 1713;  
38  
39  
40  
41 MS/ESI:  $(\text{M}+\text{H})^+$  343.0914 (m/z).  
42  
43  
44  
45

46  
47 *Synthesis of (R)-4-methylphenyl-4-[(4-methylphenoxy)carbonyl]amino-3-oxoisoxazolidine-2-*  
48  
49 *carboxylate (2b)*

50  
51 **2b** Was obtained as white crystalline solid in 75 % yield, mp 169-70°C.  $^1\text{H}$  NMR ( $\text{DMSO}-d_6$ ): 8.48  
52  
53 (bs, 1H,  $\text{D}_2\text{O}$  exchange); 7.25 (d, 2H,  $J = 7.83$  Hz); 7.19 (d, 2H,  $J = 7.58$  Hz); 7.11 (d, 2H,  $J = 7.83$   
54  
55 Hz); 7.01 (d, 2H,  $J = 7.58$  Hz); 5.01-4.94 (m, 1H); 4.78 (t, 1H,  $J = 10.55$  Hz); 4.29 (t, 1H,  $J = 8.69$   
56  
57 Hz); 2.31 (s, 3H); 2.29 (s, 3H).  $^{13}\text{C}$  NMR ( $\text{DMSO}-d_6$ ): 166.4; 154.3; 148.4; 145.8; 147.3; 135.9;  
58  
59 134.5; 130.1; 129.7; 121.3; 121.1; 69.8; 53.0; 20.4; 20.3. FT-IR ( $\text{cm}^{-1}$ ): 3339, 1788, 1737, 1713.  
60  
MS/ESI:  $(\text{M}+\text{H})^+$  371.1085 (m/z).

1  
2  
3 *Synthesis of (R)-4-methoxyphenyl-4-[[4-methoxyphenoxy]carbonyl]amino-3-oxoisoxazolidine-2-*  
4  
5 *carboxylate (2c)*

6  
7  
8 **2c** Was obtained as white crystalline solid in 70 % yield, mp 144-5°C. <sup>1</sup>H NMR (DMSO-*d*<sub>6</sub>): 8.45  
9 (1H, bs, D<sub>2</sub>O exchange); 7.16 (d, 2H, J = 7.83 Hz); 7.06 (d, 2H, J = 7.58 Hz); 6.98 (d, 2H, J = 7.83  
10 Hz); 6.93 (d, 2H, J = 7.58 Hz); 5.02-4.95 (m, 1H); 4.77 (t, 1H, J = 10.27 Hz); 4.28 (t, 1H, J = 9.23  
11 Hz); 3.76 (s, 3H); 3.75 (3H, s). <sup>13</sup>C NMR (DMSO-*d*<sub>6</sub>): 166.3; 157.3; 156.6; 156.5; 154.5; 144.0;  
12 142.8; 122.5; 122.3; 114.6; 114.3; 69.8; 55.4; 55.3; 53.0. FT-IR (cm<sup>-1</sup>): 3346, 1790, 1731, 1715.  
13 MS/ESI: (M+H)<sup>+</sup> 403.1017 (m/z).  
14  
15  
16  
17  
18  
19  
20  
21

22 *Synthesis of (R)-4-fluorophenyl-4-[[4-fluorophenoxy]carbonyl]amino-3-oxoisoxazolidine-2-*  
23  
24 *carboxylate (2d)*

25  
26  
27 **2d** Was obtained as white crystalline solid in 75 % yield, mp 179-80°. <sup>1</sup>H NMR (DMSO-*d*<sub>6</sub>): 8.65  
28 (bs, 1H, D<sub>2</sub>O exchange); 7.50 (d, 2H, J = 8.80 Hz); 7.44 (d, 2H, J = 8.80 Hz); 7.29 (d, 2H, J = 8.80  
29 Hz); 7.18 (d, 2H, J = 8.80 Hz); 5.03-4.97 (m, 1H, Hz); 4.79 (t, 1H, J = 10.52 Hz); 4.31 (t, 1H, J =  
30 8.32 Hz). <sup>13</sup>C NMR (DMSO-*d*<sub>6</sub>): 166.8; 160.0 (d, J = 243.1 Hz); 159.5 (d, J = 242.0 Hz); 154.6; 147.2  
31 (d, J = 2.7 Hz); 146.2; 146.0 (d, J = 2.7 Hz); 123.9; 123.8 (d, J = 8.7 Hz); 116.9 (d, J = 23.6 Hz); 116.4  
32 (d, J = 23.2 Hz); 70.2; 53.5. FT-IR (cm<sup>-1</sup>): 3350, 1740, 1735, 1720. MS/CI: (M+H)<sup>+</sup> 379 (m/z).  
33  
34  
35  
36  
37  
38  
39  
40

41 *Synthesis of (R)-4-chlorophenyl-4-[[4-chlorophenoxy]carbonyl]amino-3-oxoisoxazolidine-2-*  
42  
43 *carboxylate (2e)*

44  
45  
46 **2e** Was obtained as white crystalline solid in 75 % yield, mp 160-1°C. <sup>1</sup>H NMR (DMSO-*d*<sub>6</sub>): 8.65  
47 (bs, 1H, D<sub>2</sub>O exchange); 7.52 (d, 2H, J = 8.32 Hz); 7.45 (d, 2H, J = 8.32 Hz); 7.18 (d, 2H, J = 8.28  
48 Hz); 7.15 (d, 2H, J = 8.28 Hz); 5.01-4.97 (m, 1H); 4.80 (t, 1H, J = 9.52 Hz); 4.30 (t, 1H, J = 8.32  
49 Hz). <sup>13</sup>C NMR (DMSO-*d*<sub>6</sub>): 167.3; 159.7; 159.6; 155.1; 155.0; 147.7; 147.6; 124.4; 124.3; 117.5;  
50 116.8; 70.7; 53.9. FT-IR (cm<sup>-1</sup>): 3330, 1740, 1730, 1725. MS/CI: (M+H)<sup>+</sup> 412 (m/z).  
51  
52  
53  
54  
55  
56  
57  
58  
59  
60

*Synthesis of (R)-butyl-4-[[benzyloxy]carbonyl]amino-3-oxoisoxazolidine-2-carboxylate (2f)*

0.5 mmol of N-benzyloxycarbonyl-D-4-amino-3-isoxazolidinone **1f** were dissolved in 2 mL of 1M aqueous NaHCO<sub>3</sub>; at 0°C and 1.0 mmol of n-butylchloroformate was added. The resulting suspension was stirred at room temperature for 24h. The obtained white crystalline solid was separated by centrifugation, washed with cold water, dried and crystallized from benzene. Mp 170-4°C; yield 75%. <sup>1</sup>H NMR (DMSO-*d*<sub>6</sub>): 7.35 (s, 5H); 5.06 (s, 2H); 4.87-4.80 (m, 1H); 4.62 (t, 1H, J = 8.08 Hz); 4.12 (t, 2H, J = 6.12 Hz); 4.10 (t, 1H, J = 9.4 Hz); 1.61 (m, 2H); 1.35 (m, 2H); 0.88 (t, 3H, J = 7.90 Hz). <sup>13</sup>C NMR (DMSO-*d*<sub>6</sub>): 167.3; 158.0; 148.3; 143.4; 129.1; 127.6; 127.4; 66.3; 65.9; 65.2; 63.9; 31.1; 19.4; 14.4. FT-IR (cm<sup>-1</sup>): 3330, 1720, 1715, 1696. MS/CI: (M+H)<sup>+</sup> 336 (m/z).

### *Synthesis of amide derivatives 3h-i*

Cyanomethyl anion was generated by electrochemical reduction of anhydrous acetonitrile as previously reported.<sup>21</sup> Anhydrous acetonitrile, containing 0.1 M tetraethylammonium hexafluorophosphate (TEAHFP), was electrolyzed, in N<sub>2</sub> atmosphere, at 30 mA cm<sup>-2</sup> current until 1.0 Faraday per mol was consumed (calculated relatively to D-4-amino-3-isoxazolidinone); thereafter, 1.0 mmol of D-4-amino-3-isoxazolidinone were added and the solution stirred for 15 min. 1.0 mmol of alkylbromide was added and the solution was stirred for 1.5 h at room temperature. Removal of the solvent under reduced pressure gave a crude solid that was extracted with three portions of Et<sub>2</sub>O and the combined organic extracts were dried over anhydrous Na<sub>2</sub>SO<sub>4</sub> and evaporated under reduced pressure to give a crude residue that was used, without further purification, for the synthesis of amides **3h,i**.

The crude residue (**4h** or **4i**) was dissolved in 20 mL of CHCl<sub>3</sub> and 1.2 mmol of TEA and 1.2 mmol of 3-(trifluoromethyl)benzoyl chloride were added. The obtained solution was stirred at room temperature for 24h. The solution was washed with saturated Na<sub>2</sub>CO<sub>3</sub>, dried over anhydrous Na<sub>2</sub>SO<sub>4</sub> and removed under reduced pressure; the obtained residue was purified on silica gel column chromatography to afford pure **3h** and **3i**.

1  
2  
3 N-[2-(n-octyl)-3-oxoisoxazolidin-4-yl]-3-(trifluoromethyl)benzamide (**3h**) was purified on silica gel  
4 column (CH<sub>2</sub>Cl<sub>2</sub>/ ethyl acetate, 9:1). Mp 95-6°C; yield 70%. <sup>1</sup>H NMR (DMSO-*d*<sub>6</sub>): 9.28 (bs,1H,  
5 D<sub>2</sub>O exchange); 8.22 (m, 1H, J = 1.78 Hz); 8.18 (dd,1H, J = 7.71 Hz, J = 1.58 Hz); 7.95 (dd, 1H, J =  
6 7.91 Hz, J = 2.09 Hz); 7.74 (m, 1H); 5.09 (m,1H, J = 10.15 Hz); 4.61 (t,1H, J = 8.56 Hz); 4.11 (t,  
7 1H, J = 8.68 Hz); 3.50 (d, 2H, J = 7.25 Hz); 1.56 (m, 2H); 1.26 (m, 10H); 0.85 (3H, t, J = 7.00 Hz).  
8 <sup>13</sup>C NMR (DMSO-*d*<sub>6</sub>): 166.8; 165.4; 134.7; 132.1; 130.3; 130.0 (q, J=32.4 Hz); 128.7; 125.8; 124.4;  
9 70.2; 52.3; 45.2; 31.7; 29.0; 28.9; 26.8; 26.5; 22.5; 14.4. FT- IR (cm<sup>-1</sup>): 3301, 1671, 1662. MS/CI:  
10 (M+H)<sup>+</sup> 387 (m/z).  
11  
12

13  
14  
15 N-[2-(2,6-dichlorobenzyl)-3-oxoisoxazolidin-4-yl]-3-(trifluoromethyl)benzamide (**3i**) was purified  
16 on silica gel column (CH<sub>2</sub>Cl<sub>2</sub> / ethyl acetate, 9:1).Mp 162-4°C; yield 75%. <sup>1</sup>H NMR (DMSO-*d*<sub>6</sub>):  
17 7.99 (bs,1H, D<sub>2</sub>O exchange); 7.80 (m,1H, J = 1.58 Hz); 7.74 (dd, 1H, J = 7.55 Hz, J = 1.68 Hz);  
18 7.59 (dd, 1H, J = 6.77 Hz, J = 1.98 Hz); 7.37 ( m, 1H); 7.27 (t, 2H, J = 6.30 Hz);7.24 (d, 2H); 5.15  
19 (s, 2H); 4.97 (m, 1H, J = 9.87 Hz); 4.87 (dd,1H, J = 8.33 Hz); 3.98 (t, 1H, J = 8.68 Hz). <sup>13</sup>C NMR  
20 (DMSO-*d*<sub>6</sub>): 166.6; 166.1; 136.9; 133.6; 131.1 (q, J=32.9) ; 130.7; 129.2; 129.1; 128.7; 128.6;  
21 125.2; 124.7; 72.8; 52.8; 44.7.FT- IR (cm<sup>-1</sup>): 3253, 1713, 1635. MS/CI: (M+H)<sup>+</sup> 433 (m/z).  
22  
23  
24  
25  
26  
27  
28  
29  
30  
31  
32  
33  
34  
35  
36  
37  
38  
39  
40

### 4.3 Microbiology

41  
42  
43 The biological activity of the synthesized compounds has been evaluated as reported elsewhere<sup>24</sup>  
44 toward *M. tuberculosis* H37Rv ATCC 27294.  
45  
46  
47  
48  
49

### Acknowledgments

50  
51 We thank Dr. Roberto Cirilli (Dipartimento del Farmaco, Istituto Superiore di Sanità, Rome, Italy)  
52 for the chiral HPLC analysis. We also thank Prof. A. De Logu from “*Dipartimento di Scienze e*  
53 *Tecnologie Biomediche*”, University of Cagliari for the biological activity data. One of us (F.B.)  
54 acknowledge Sapienza Università di Roma (grant “Progetti per Avvio alla Ricerca” prot.  
55 C26N12JZCT).  
56  
57  
58  
59  
60

## References

1. WHO Global tuberculosis report 2012.  
[http://www.who.int/tb/publications/global\\_report/en/index.html](http://www.who.int/tb/publications/global_report/en/index.html)
2. Ehlers, S., Lazy, dynamic or minimally recrudescant? On the elusive nature and location of the mycobacterium responsible for latent tuberculosis. *Infection* **2009**, 37, 87-95.
3. Di Perri, G.; Bonora, S., Which agents should we use for the treatment of multidrug-resistant Mycobacterium tuberculosis? *J Antimicrob Chemother* **2004**, 54, 593-602.
4. Velayati, A. A.; Masjedi, M. R.; Farnia, P.; Tabarsi, P.; Ghanavi, J.; Ziazarifi, A. H.; Hoffner, S. E., Emergence of new forms of totally drug-resistant tuberculosis bacilli: super extensively drug-resistant tuberculosis or totally drug-resistant strains in iran. *Chest* **2009**, 136, 420-5.
5. Udwadia, Z. F.; Amale, R. A.; Ajbani, K. K.; Rodrigues, C., Totally drug-resistant tuberculosis in India. *Clinical infectious diseases : an official publication of the Infectious Diseases Society of America* **2012**, 54, 579-81.
6. Guy, E. S.; Mallampalli, A., Managing TB in the 21st century: existing and novel drug therapies. *Thorax* **2008**, 63, 401-8.
7. Bhowruth, V.; Dover, L. G.; Besra, G. S., Tuberculosis chemotherapy: recent developments and future perspectives. *Prog Med Chem* **2007**, 45, 169-203.
8. Piccaro, G.; Filippini, P.; Giannoni, F.; Scipione, L.; Tortorella, S.; De Vita, D.; Mellini, P.; Fattorini, L., Activity of drugs against dormant Mycobacterium tuberculosis. *J Chemother* **2011**, 23, 175-8.
9. Ragno, R.; Marshall, G. R.; Di Santo, R.; Costi, R.; Massa, S.; Rompei, R.; Artico, M., Antimycobacterial pyrroles: synthesis, anti-Mycobacterium tuberculosis activity and QSAR studies. *Bioorg Med Chem* **2000**, 8, 1423-32.
10. Biava, M.; Porretta, G. C.; Poce, G.; Supino, S.; Deidda, D.; Pompei, R.; Molicotti, P.; Manetti, F.; Botta, M., Antimycobacterial agents. Novel diarylpyrrole derivatives of BM212 endowed with high activity toward Mycobacterium tuberculosis and low cytotoxicity. *Journal of medicinal chemistry* **2006**, 49, 4946-52.

- 1  
2  
3 11. Ballante, F.; Ragno, R., 3-D QSAutogrid/R: an alternative procedure to build 3-D QSAR models.  
4  
5 Methodologies and applications. *J Chem Inf Model* **2012**, 52, 1674-85.  
6  
7  
8 12. Manetti, F.; Corelli, F.; Biava, M.; Fioravanti, R.; Porretta, G. C.; Botta, M., Building a pharmacophore  
9  
10 model for a novel class of antitubercular compounds. *Farmaco* **2000**, 55, 484-91.  
11  
12 13. Barnum, D.; Greene, J.; Smellie, A.; Sprague, P., Identification of common functional configurations  
13  
14 among molecules. *J Chem Inf Comput Sci* **1996**, 36, 563-71.  
15  
16  
17 14. BIAVA; Mariangela; FIORAVANTI; Rossella; PORRETTA; Cesare, G.; DEIDDA; Delia; LAMPIS; Giorgio;  
18  
19 POMPEI; Raffaello; TAFI; Andrea; MANETTI; Fabrizio, New derivatives of toluidine: Synthesis, antitubercular  
20  
21 activity and pharmacophore hypothesis. *Med. Chem. Res* **2002**.  
22  
23  
24 15. Biava, M.; Porretta, G. C.; Poce, G.; De Logu, A.; Saggi, M.; Meleddu, R.; Manetti, F.; De Rossi, E.;  
25  
26 Botta, M., 1,5-Diphenylpyrrole derivatives as antimycobacterial agents. Probing the influence on  
27  
28 antimycobacterial activity of lipophilic substituents at the phenyl rings. *Journal of medicinal chemistry* **2008**,  
29  
30 51, 3644-8.  
31  
32  
33 16. Biava, M.; Porretta, G. C.; Deidda, D.; Pompei, R.; Tafi, A.; Manetti, F., Antimycobacterial  
34  
35 compounds. New pyrrole derivatives of BM212. *Bioorganic & medicinal chemistry* **2004**, 12, 1453-8.  
36  
37  
38 17. Biava, M.; Porretta, G. C.; Poce, G.; Deidda, D.; Pompei, R.; Tafi, A.; Manetti, F., Antimycobacterial  
39  
40 compounds. Optimization of the BM 212 structure, the lead compound for a new pyrrole derivative class.  
41  
42 *Bioorganic & medicinal chemistry* **2005**, 13, 1221-30.  
43  
44  
45 18. Biava, M.; Cesare Porretta, G.; Deidda, D.; Pompei, R.; Tafi, A.; Manetti, F., Importance of the  
46  
47 thiomorpholine introduction in new pyrrole derivatives as antimycobacterial agents analogues of BM 212.  
48  
49 *Bioorganic & medicinal chemistry* **2003**, 11, 515-20.  
50  
51  
52 19. Biava, M.; Porretta, G. C.; Poce, G.; De Logu, A.; Meleddu, R.; De Rossi, E.; Manetti, F.; Botta, M.,  
53  
54 1,5-Diaryl-2-ethyl pyrrole derivatives as antimycobacterial agents: design, synthesis, and microbiological  
55  
56 evaluation. *Eur J Med Chem* **2009**, 44, 4734-8.  
57  
58  
59 20. Stammer, C. H.; Kartha, C. C.; Chaturvedi, N. C.; McKinney, J. D., Cycloserine derivatives. *Journal of*  
60  
*medicinal chemistry* **1970**, 13, 1013-5.

- 1  
2  
3 21. Feroci, M.; De Vita, D.; Scipione, L.; Sotgiu, G.; Tortorella, S., Electrogenerated acetonitrile anion  
4 induced selective N-alkylation of bifunctional compounds. *Tetrahedron Letters* **2012**, 53, 2564-2567.  
5  
6  
7 22. Jain, A. N., Ligand-based structural hypotheses for virtual screening. *Journal of medicinal chemistry*  
8 **2004**, 47, 947-61.  
9  
10 23. Morris, G. M.; Huey, R.; Lindstrom, W.; Sanner, M. F.; Belew, R. K.; Goodsell, D. S.; Olson, A. J.,  
11 AutoDock4 and AutoDockTools4: Automated docking with selective receptor flexibility. *J Comput Chem*  
12 **2009**, 30, 2785-91.  
13  
14 24. Castagnolo, D.; De Logu, A.; Radi, M.; Bechi, B.; Manetti, F.; Magnani, M.; Supino, S.; Meleddu, R.;  
15 Chisu, L.; Botta, M., Synthesis, biological evaluation and SAR study of novel pyrazole analogues as inhibitors  
16 of Mycobacterium tuberculosis. *Bioorg Med Chem* **2008**, 16, 8587-91.  
17  
18  
19  
20  
21  
22  
23  
24  
25  
26  
27  
28  
29  
30  
31  
32  
33  
34  
35  
36  
37  
38  
39  
40  
41  
42  
43  
44  
45  
46  
47  
48  
49  
50  
51  
52  
53  
54  
55  
56  
57  
58  
59  
60

1  
2  
3 **Pharmacophore Assessment Through 3-D QSAR:evaluation of the predictive ability on new**  
4 **derivatives by the application on a serie of antitubercularagents.**  
5  
6  
7  
8

9  
10 Laura Friggeri, Flavio Ballante,\* Rino Ragno,\* Ira Musmuca, Daniela De Vita, Fabrizio Manetti,  
11 Mariangela Biava, Luigi Scipione, Roberto Di Santo, Roberta Costi, Marta Feroci and Silvano  
12 Tortorella.  
13

